

GW170817 and GW190425 as Hybrid Stars of Dark and Nuclear Matters

Kilar Zhang*, Guo-Zhang Huang[†], Feng-Li Lin[‡]

Department of Physics, National Taiwan Normal University, Taipei 11677, Taiwan

Abstract

We propose three scenarios for compact hybrid stars consisting of nuclear and dark matters which could possibly serve as alternative interpretations to the LIGO/Virgo events GW170817 and GW190425. To demonstrate our proposal, we adopt the SLy4 equation of state (EoS) for nuclear matter, and an EoS for a bosonic self-interacting dark matter (SIDM), which is simple and capable of yielding both reasonable halo density and compact stars. We study the mass-radius and tidal Love number (TLN)-mass relations for these compact hybrid stars, and also generalize the Bardeen-Thorne-Meltzer (BTM) criteria to discuss in details the possible saddle instability due to the nature of two-fluid model. Our results show that it is possible for our hybrid star scenarios to explain GW170817 and GW190425. Some of the hybrid stars can have compact neutron or mixed cores around 10km while possessing thick dark matter shells, which can then explain the astrophysical observations of neutron stars with compact photon radius and mass higher than 2 solar masses. Reversely, we also infer the dark matter model from the parameter estimation of GW190425. Our scenarios of compact hybrid stars can be further tested by the coming LIGO/Virgo O3 events.

*kilar.zhang@gmail.com

[†]60641027s@ntnu.edu.tw

[‡]linfl@gapps.ntnu.edu.tw

Corresponding Author

Contents

1	Introduction	2
2	Model of equation of state for dark and nuclear matters	4
3	Tolman-Oppenheimer-Volkoff configuration and tidal Love number	5
4	M-R and Λ-M relations	7
4.1	For Scenario I and II:	7
4.2	For Scenario III:	9
5	Fitting of GW170817 and GW 190425	12
6	Parameter estimation for EoS of dark matter	13
7	Conclusion	15

1 Introduction

Dark matter, though prevails over the universe and consists of about 3-quarter of matter content, reveals little evidence in the direct search in the past three decades (Klasen et al. 2015; Akerib et al. 2017; Cui et al. 2017; Aprile et al. 2017). However, it is hard to detect the dark matter directly by the conventional electromagnetic means due to its rare interaction with the visible sector. On the other hand, everything gravitates. If dark matter can form the compact binary coalescences (CBC), one can detect the associated gravitational waves (GW) to infer its equation of state (EoS) and the corresponding microscopic theory of dark matter (Kouvaris & Nielsen 2015; Maselli et al. 2017; Sennett et al. 2017). This can be thought as an alternative direct search through the relation between gravitational astronomy, microscopic and macroscopic physics of dark matter. The most popular model for dark matter is the WIMP (weakly interacting massive particles) (Jungman et al. 1996). Despite that, the WIMP cannot well explain some astrophysical properties of dark matter halo, such as the smooth core profile or the missing satellites. It motivates to introduce SIDM (the self-interacting dark matter) to resolve these issues (Spergel & Steinhardt 2000; Rocha et al. 2013; Peter et al. 2013; Kaplinghat et al. 2016). Moreover, it has been shown (Colpi et al. 1986; Schunck & Mielke 2003; Eby et al. 2016; Deliyergiyev et al. 2019) that some bosonic models of SIDM can yield compact stars of few solar masses, the so-called dark stars.

Given the possibilities of compact dark stars, one can speculate the existence of compact hybrid stars made of both dark and nuclear matters. This is the analogue to the dark halos made of dark and visible matters (Battaglia et al. 2005) but in a much smaller scale. There are three scenarios of compact hybrid stars as shown in Fig. 1, which depend on how dark and nuclear matters interact, and also on the accretion mechanism. The scenario I is to have the stars with neutron core and dark matter shell, and the scenario II is for the stars with dark matter core and neutron shell. For both scenarios we assume there is interaction between dark and nuclear matters, or spontaneous symmetry breaking to form a domain

wall separating the core and shell ¹. Otherwise, it will lead to the scenario III for which the dark and nuclear matters are mixed inside the core but with only one component in the shell. Some hybrid stars of scenario IIIa and IIIb have been proposed and studied in (Nelson et al. 2019) and (Ellis et al. 2018), respectively. These hybrid stars can be seen as the cousins of neutron stars with the new parameter r_W characterizing the radius of the inner core. Here, we simply assume the existence of these hybrid stars and leave their formation mechanism for future studies.²

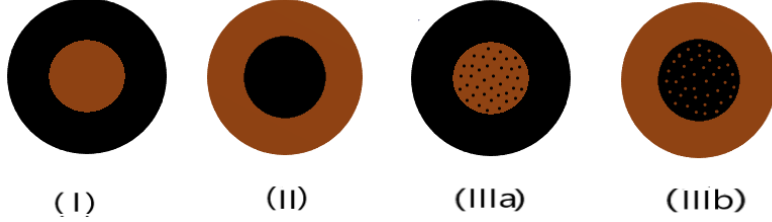


Figure 1: Three scenarios of hybrid stars. Black color denotes dark matter and brown color denotes nuclear matter. For scenario I the star consists of a pure nuclear matter core and a pure dark matter shell, and for scenario II it consists of a pure dark matter core and a pure nuclear matter shell. For scenario III, we have a mixed core and either a pure dark matter shell (IIIa) or a pure nuclear matter one (IIIb). They can form the systems of binary hybrid stars (BHS).

Despite the speculated hybrid stars, it is hard to detect them due to either lack of electromagnetic signals or not enough telling from the neutron stars. However, these hybrid stars will have different mass-radius relation and the tidal deformability which can be encoded in the GW emitted from the coalescences of binary hybrid stars (BHS). Thus, we may test the above three scenarios for BHS via GW events discovered by LIGO/Virgo. Currently, there are two observed events usually identified as binary neutron stars (BNS), namely, GW170817 (Abbott et al. 2017, 2019) and GW190425 (Abbott et al. 2020a). The key feature of both events is their low tidal Love numbers (TLNs). Moreover, the total mass and the associated component masses of GW190425 seem larger than the ones expected for the neutron stars, in comparison to GW170817. Although these events ³ cannot serve as evidences of the existence of new astronomical objects, they do not deny alternative explanation such as the one provided here by the scenarios of hybrid stars. We hope that future observations will scrutinize these scenarios. Reversely, we can constrain the dark matter model by analyzing the astrophysical properties of the hybrid stars from the GW data.

¹In a recent paper (Gresham & Zurek 2019), it shows that a domain wall can form even for very small interaction between dark and nuclear matter. Once the nuclear and dark matters are separated by a domain wall, one can solve the TOV equations separately within each phase, and then match the results by some proper junction conditions. In this way, the mixed phase rule is only needed to determine the size of the core given a specific model interaction between dark matter and baryons. However, in this paper we will treat the size of the core as a parameter and bypass the phase rule.

²The capture rate of dark matter by neutron star is too small to form sizable share in the hybrid stars due to the negligible interaction between dark matter and baryons (Kouvaris & Tinyakov 2011; McDermott et al. 2012). However, there are proposals to dramatically increase the cross-section by forming the nuggets (Gresham et al. 2017, 2018b,a; Coskuner et al. 2019) so that the capture rate could be accelerated. Another possibility for quickly accumulating dark matters is through the Bondi accretion (Edgar 2004).

³Including the new event GW190814 (Abbott et al. 2020b) after completion of this paper.

The organization of the paper is as follows: In Section 2 we introduce the EoSs for the models used for dark and nuclear matters; Section 3 shows TOV configurations and how to calculate tidal Love number; Section 4 illustrates M - R and Λ - M relations from our numerical results; In Section 5 we fit GW170817 and GW 190425 using our model; Section 6 describes parameter estimation for EoS of dark matter; Section 7 is the conclusion.

2 Model of equation of state for dark and nuclear matters

In this paper, we will show that both GW170817 and GW190425 can be easily explained by a simple toy model of hybrid stars based on the above three scenarios. We do not aim to pin down the models for nuclear and dark matters, but to demonstrate the viability of the hybrid star scenarios. There are many bosonic dark matter model candidates, some of which predict light dark matter particle such as axion (Kuster et al. 2008). However, if the dark matter is too light, it is not easy to form compact stars (Eby et al. 2019) but the cloud around a compact star or black hole (Hannuksela et al. 2019).

For our purpose of searching for the compact stars of few solar masses, it is more natural to choose the heavier dark matter with mass around MeV to GeV. It had been shown that the WIMP may not be able to yield smooth dark halo profile but needs to introduce some self-interaction to fix the issue (Spergel & Steinhardt 2000; Rocha et al. 2013; Peter et al. 2013; Kaplinghat et al. 2016). Thus, we consider a simple model of nuclear and dark matters. We adopt the SIDM of a bosonic scalar field ϕ with potential $m^2\phi^2 + \frac{\lambda}{4}\phi^4$. Moreover, we consider the model in the regime $\lambda M_{\text{planck}}^2/m^2 \gg 1$ so that it can be equivalently described by a hydrodynamical perfect fluid with EoS given by (Colpi et al. 1986)

$$\rho/\rho_\odot = 3 (p/p_\odot) + \mathcal{B} (p/p_\odot)^{1/2}, \quad (1)$$

where $\mathcal{B} \sim \frac{0.08}{\sqrt{\lambda}} (\frac{m}{\text{GeV}})^2$ is a free parameter⁴. In this paper we will adopt the astrophysical units:

$$r_\odot = G_N M_\odot / c^2, \quad \rho_\odot = M_\odot / r_\odot^3, \quad p_\odot = c^2 \rho_\odot,$$

for the (half) Schwarzschild radius of the Sun, the corresponding energy density and pressure, respectively. Note that M_\odot denotes the solar mass, and G_N the Newton constant.

For this SIDM to also explain the smooth density profile of dark halos, one needs to impose the constraint on the cross section of self-scattering, which is translated into a tiny window for λ (Kaplinghat et al. 2016):

$$30 (\frac{m}{\text{GeV}})^{3/2} < \lambda < 90 (\frac{m}{\text{GeV}})^{3/2}. \quad (2)$$

Therefore, if we can pin down the parameter \mathcal{B} from the GW events, we can almost determine the parameters of this SIDM.

⁴This EoS is slightly below the “sound barrier”, which means the derived sound speed is always below the con formal limit, i.e., $1/\sqrt{3}$ of the light speed, and it takes the same form as the conjectured EoS of quark matter in the deep core of neutron star (Hoyos et al. 2016; Annala et al. 2018). The coincidence is due to the ϕ^4 potential and the nearly massless nature of quarks in the high chemical potential limit. If one consider higher ϕ^n with $n > 4$, the resultant EoS can break sound barrier (Zhang & Lin 2020).

As a first step, in this paper we only consider bosonic SIDM, however, the fermionic SIDM with Yukawa coupling constrained by the observed dark halo profile should be also viable for the formation of compact hybrid stars. For example, in (Kouvaris & Nielsen 2015; Maselli et al. 2017) the EoS for this kind of fermionic SIDM has been obtained and used to study the compact star configurations, see also the recent paper (Gresham & Zurek 2019) for the hybrid stars with a more complicated fermionic SIDM. One can follow the same procedure of this paper to consider the compact hybrid stars with fermionic SIDM.

As for the nuclear matter, there are also many candidate models with different EoSs. One type is the phenomenological model like the SLy4 (Douchin & Haensel 2001)⁵ used extensively in gravitational wave data analysis (Abbott et al. 2017, 2019, 2020a). The other type is derived theoretically, like the one in (Zhang et al. 2020) from a well-motivated holographic quantum chromodynamics model, i.e., Sakai-Sugimoto model (Sakai & Sugimoto 2005a,b; Hata et al. 2007). Since the phenomenological model is more generally accepted, we choose the SLy4 model for the discussion.

3 Tolman-Oppenheimer-Volkoff configuration and tidal Love number

The GW of CBC encodes the component masses $M_{1,2}$, and also the TLNs $\Lambda_{1,2}$ in the following combined quantity

$$\tilde{\Lambda} = \frac{16}{13} \frac{(M_1 + 12M_2)M_1^4\Lambda_1 + (M_2 + 12M_1)M_2^4\Lambda_2}{(M_1 + M_2)^5}. \quad (3)$$

Note that $\tilde{\Lambda} = (\Lambda_1 + \Lambda_2)/2$ for $M_1 = M_2$. For each hybrid star scenario, we have two model parameters \mathcal{B} and r_W . We shall connect the model parameters to the inferred quantities from observation data by the mass-radius and TLN-mass relations.

Given a set of (\mathcal{B}, r_W) we first obtain the mass-radius relation by solving the Tolman-Oppenheimer-Volkoff (TOV) equations (Tolman 1939; Oppenheimer & Volkoff 1939) for multi-component cases (Mukhopadhyay et al. 2017; Rezaei 2018) using units $G = c = 1$:

$$p'_I = -(\rho_I + p_I)\phi', \quad m'_I = 4\pi r^2 \rho_I, \quad \phi' = \frac{m + 4\pi r^3 p}{r(r - 2m)}, \quad (4)$$

where $' := \frac{d}{dr}$, $I = D$ or N , the mass inside radius r is $m(r) = \sum_I m_I$, pressure $p = \sum_I p_I$, energy density $\rho = \sum_I \rho_I$ by summing the contributions from both dark matter ($I = D$) and nuclear matter ($I = N$), and the Newton potential $\phi := \frac{1}{2} \ln(-g_{tt})$ with g_{tt} the tt -component of the metric. The size R of the star is determined by $p(r = R) = 0$, and the mass of the star is given by $m(R)$. For the first scenario, we set $p_D = \rho_D = 0$ and use EoS SLy4 to solve TOV equations for $r \leq r_W$. For $r \geq r_W$ we set $p_N = \rho_N = 0$ and set initial value of p_D at r_W equal to $p_N(r_W)$, then use (1) to solve the TOV equations until $r = R$. For the second scenario we do the same thing by swapping the roles of dark and nuclear matters. For the third scenario, we tune the initial values at $r = 0$ for both p_D and p_N and use both (1) and EoS SLy4 to solve TOV. In this case r_W is determined by the first vanishing p_I , then we solve the TOV equations for $r > r_W$ until $r = R$ for the remaining nonvanishing p_I component.

⁵<https://compose.obspm.fr/eos/134>

Naively, one can sum (4) over the components to get a set of single-fluid TOV equations. However, the EoS for each component is usually not in the linear form, it is then impossible to form a EoS of single fluid, namely $\rho = \sum_I \rho_I \neq \rho(p)$. This requires to impose initial condition for each component when solving the TOV, and leads to the subtlety discussed right below when considering the stability of the hybrid stars of the third scenario based on the generalization of the Bardeen-Thorne-Meltzer (BTM) criteria (Bardeen et al. 1966).

A key difference between first two scenarios and the third one is the stability issues. For the first two, we have just one initial-value parameter for solving TOV, i.e., either $p_D(0)$ or $p_N(0)$, but have both for the third one, thus the stability issue of the latter is more tricky due to possible saddle instability.

Another issue is regarding the determination of r_W . It seems that r_W is a free parameter in scenario I and II, but can be determined automatically in scenario III. This however is not true. For scenario I and II to have a domain wall separating the dark matter and baryonic phases, there should have model interactions between these two components, which will then build up the chemical equilibrium among them. This implies some mixed phase rule should be applied to determine r_W . Therefore, even in scenario I and II r_W is not a free parameter. Despite that, it needs to specify the model interaction to determine r_W unambiguously, such as the example in (Gresham & Zurek 2019). In this work we will not consider scenario I and II for some particular model interactions, instead we choose r_W as a parameter to characterize the model interactions between dark matter and baryons.

After having solved the stable TOV configurations, we solve the linear perturbation around them to extract the TLN, denoted by Λ and defined by

$$Q_{ab} = -M^5 \Lambda \mathcal{E}_{ab} \quad (5)$$

where M is the mass of the star, Q_{ab} is the induced quadrupole moment, and \mathcal{E}_{ab} is the external gravitational tidal field strength. As shown in (Hinderer 2008; Postnikov et al. 2010), to obtain Λ , we first need to solve the following equation for $y(r) := rH'(r)/H(r)$ with $H(r)$ the linear perturbation of g_{tt} around a TOV configuration:

$$ry' + y^2 + P(r)y + r^2Q(r) = 0 \quad (6)$$

with boundary condition $y(0) = 2$ and

$$P = (1 + 4\pi r^2(p - \rho))/(1 - 2m/r), \quad (7)$$

$$Q = 4\pi(5\rho + 9p + \sum_I \frac{\rho_I + p_I}{dp_I/d\rho_I} - \frac{6}{4\pi r^2})/(1 - 2m/r) - 4\phi'^2. \quad (8)$$

Moreover, when we consider a hybrid star with two separated phases like the first two scenarios, the TOV and tidal equations must be solved separately and connect with correct junction conditions on the domain wall. The pressure p is continuous but the energy density ρ is not, so that y encounters a jump around the domain wall. The required junction conditions are sketched below, for more details see (Postnikov et al. 2010).

Suppose the pressure reads p_W on the domain wall located at $r = r_W$, which separates the two phases. The sound speed in the vicinity of a density discontinuity is

$$\frac{d\rho}{dp} = \frac{1}{c_s^2} = \frac{d\rho}{dp} \Big|_{p \neq p_W} + \Delta\rho_p \delta(p - p_W), \quad (9)$$

where $\Delta\rho_p = \rho(p_W + 0) - \rho(p_W - 0)$ is the energy density jump across p_W . Yet since p decreases as r increases, equivalently $\Delta\rho_p = -(\rho(r_W + 0) - \rho(r_W - 0)) \equiv -\Delta\rho$.

When integrating (6) near the domain wall at $r = r_W$, most of the terms give zero, and only the terms proportional to the δ -function can contribute. Therefore, this then results in

$$ry'(r)|_{r=r_W} + r^2 4\pi e^{\lambda(r)} (\rho(r) + p(r)) \frac{d\rho}{dp}|_{r=r_W} = 0. \quad (10)$$

Since $\frac{d\rho}{dp} = \frac{d\rho}{dr} \frac{1}{dp/dr}$, where $\frac{dp}{dr}$ can be read off from the first TOV equation (4), and $\frac{d\rho}{dr}|_{r=r_W} = \Delta\rho\delta(r - r_W)$, we obtain that ⁶

$$\Delta y = \frac{\Delta\rho}{p + m(r_W)/(4\pi r_W^3)}, \quad (11)$$

where $\Delta y \equiv y(r_W + 0) - y(r_W - 0)$. As a result, we can solve the TOV and tidal deformation equations with the above junction conditions for the scenarios I and II.

Once (6) is solved, the TLN Λ can be obtained through an algebraic expression of $y_R \equiv y(R)$ and the “compactness” $C = M/R$ given by (Hinderer 2008; Postnikov et al. 2010)

$$\begin{aligned} \Lambda = & \frac{16}{15} (1 - 2C)^2 [2 + 2C(y_R - 1) - y_R] \times \left\{ 2C(6 - 3y_R + 3C(5y_R - 8)) \right. \\ & + 4C^3 [13 - 11y_R + C(3y_R - 2) + 2C^2(1 + y_R)] \\ & \left. + 3(1 - 2C)^2 [2 - y_R + 2C(y_R - 1)] \log(1 - 2C) \right\}^{-1}. \end{aligned} \quad (12)$$

4 M - R and Λ - M relations

Based on the above we evaluate the M - R and Λ - M relations for the three hybrid star scenarios with dark matter EoS given by (1) and the nuclear matter EoS given by SLy4.

4.1 For Scenario I and II:

We consider the case with the SLy4 EoS for nuclear matter. In Fig. 2 we show the M - R relations for the first two scenarios for $\mathcal{B} = 0.035$ (with various r_W labelled as **aRN** for the first scenario, and as **aRD** for the second) or $\mathcal{B} = 0.055$ (labelled by **bRN** and **bRD**), and in Fig. 3 we show the corresponding Λ - R relations. From the results we observe the followings. (i) The one labelled by **aRD**=0 (and **bRD**=0) is the pure neutron stars which can both fit GW170817 and the traditional astronomical observations. As the dark matter core increases its size, the maximal mass goes down first as the boson EoS is less stiff, then go up as the allowed maximal mass of boson EoS is higher, and at the same time the total radius becomes larger. (ii) For the first scenario, we see that there is a jump around **aRN**=9.5 or **bRN**=7 (though the latter not shown explicitly in Fig. 2) beyond which the small-radius configurations become unstable (indicated by dash line in Fig. 2), this may imply some first order phase transition. On the other hand, above this critical **RN**, there are more compact hybrid stars which can be consistent with LIGO observation with small TLN as indicated in Fig. 3. (iii) The configuration with M larger than $3M_\odot$ are mainly composed by dark matters as seen from the ratio of r_W/R . Contrarily, the more compact

⁶There are typos in the counterpart of (11) in (Postnikov et al. 2010).

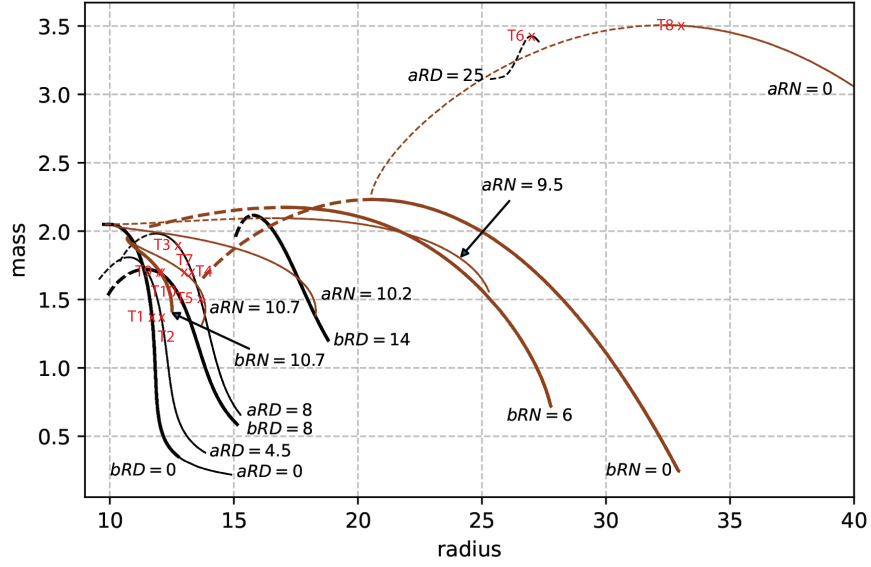


Figure 2: Mass-Radius relations for the hybrid stars of type (I) and (II) in Fig. 1, which are made of nuclear matter of SLy4 EoS and dark matter of EoS (1) with $\mathcal{B} = 0.035$ or 0.055 . With $\mathcal{B} = 0.035$ these relations are labelled by **aRN** = r_W (brown) for the first scenario, by **aRD** = r_W (black) for the second. Similarly, with $\mathcal{B} = 0.055$ they are labelled by **bRN** = r_W (brown) and **bRD** = r_W (black)). For example, **aRD**=8 means the radius of dark core is 8km, with $\mathcal{B} = 0.035$. The unstable configurations are indicated by the parts of dashed lines. Note that r_W is a parameter to characterize the model interaction between dark matter and baryons.

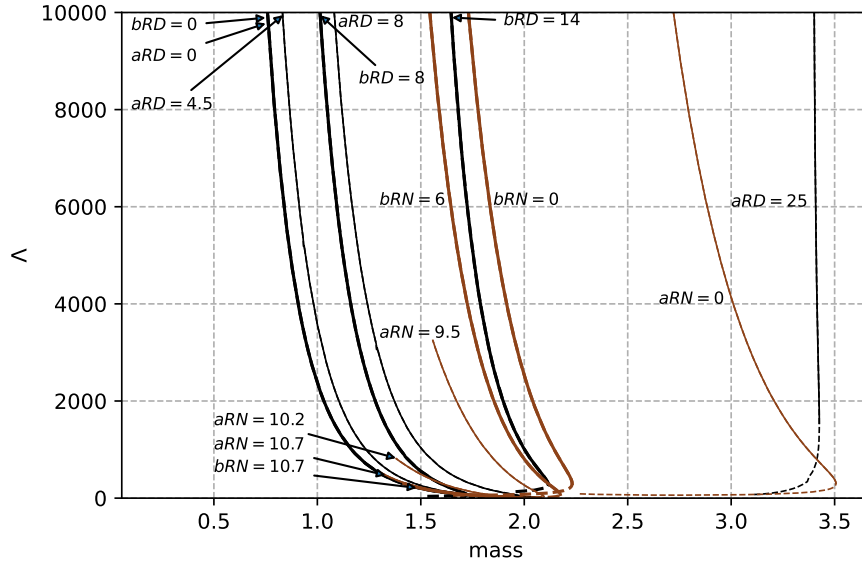


Figure 3: Corresponding TLN-Mass relations of Fig. 2. Similarly, the unstable configurations are indicated by the parts of dashed lines.

hybrid stars of smaller R are mainly composed by nuclear matters. This is understandable since the SLy4 EoS is stiffer than EoS (1). It then implies that the final state of the most binary hybrid stars' mergers are unstable unless the initial stars are almost pure dark stars. Thus, if the component stars of GW190425 are the hybrid stars of these two scenarios, the final state will collapse into a black hole.

In a short summary: in general, due to the additional component of matters, our hybrid stars can host a wider range of masses and TLNs than pure neutron stars or dark stars. This will then be taken as the special feature to distinguish from the pure neutron and dark stars of a given EoS in the forthcoming GW observational data.

Finally, we should remind the readers that in scenario I and II, r_W should be determined by a given model interaction between dark matter and baryons. Therefore, our results can be thought as tabulating the possible configurations of scenario I and II for generic model dark matter-baryon interactions.

4.2 For Scenario III:

Next, we show the M - R and Λ - M relations for the third scenario of hybrid stars, namely the mixed ones in the core, and the associated star configurations are denoted by **BMX** for $B = 0.055$ of dark matter EoS and for either SLy4 EoS or Holo one (in the appendix) of nuclear matter. In Fig. 4 we show the results for SLy4.

Unlike the first two scenarios, there are saddle instabilities for the third scenario. Here we like to elaborate on the criterion for judging the stable regions. A simple way of determining the stable region is the so-called BTM (Bardeen-Thorne-Meltzer) criteria ⁷ (Bardeen et al. 1966) as follows: We start with the stable configuration with very low core pressure, and trace along the M - R curve by increasing the core pressure. Then, when passing through an extremum on the M - R curve, we can have the following two situations: (1) If the M - R curve bends counterclockwise, a stable mode will become unstable; (2) Otherwise, one unstable mode become stable. By this way, we can determine which part on the M - R curve admits stable configurations.

However, in most of the cases we will not solve the M - R curve from the the very low core pressure, such as the case considered here. To determine the stability of the regime interested, we can assume the stability/instability of a certain part of the M - R curve, and then apply the BTM criteria reversely as follows,

Reverse BTM Stability Criteria: when passing through each extremum of the M - R curve in the direction of decreasing the core pressure,

1. if the M - R curve bends clockwise, one unstable mode becomes stable;
2. Otherwise, one stable mode becomes unstable.

After that, we can apply the BTM criteria on the same regime for consistency check to determine the stability/instability of the initial part. Some examples for the above practice are shown in Fig. 5 where the solid lines denote the stable regions, and the dotted parts the unstable ones. The arrows indicate the direction of increasing core pressure. Note that curves O - A - B - C and O' - A' - D' - B' - C' look quite similar but differ by the extremum D' . Thus, they have quite different stability/instability structures after applying the above

⁷This was shown in (Bardeen et al. 1966) to be equivalent to the stability analysis by solving the Sturm-Liouville eigenmodes of radial oscillation.

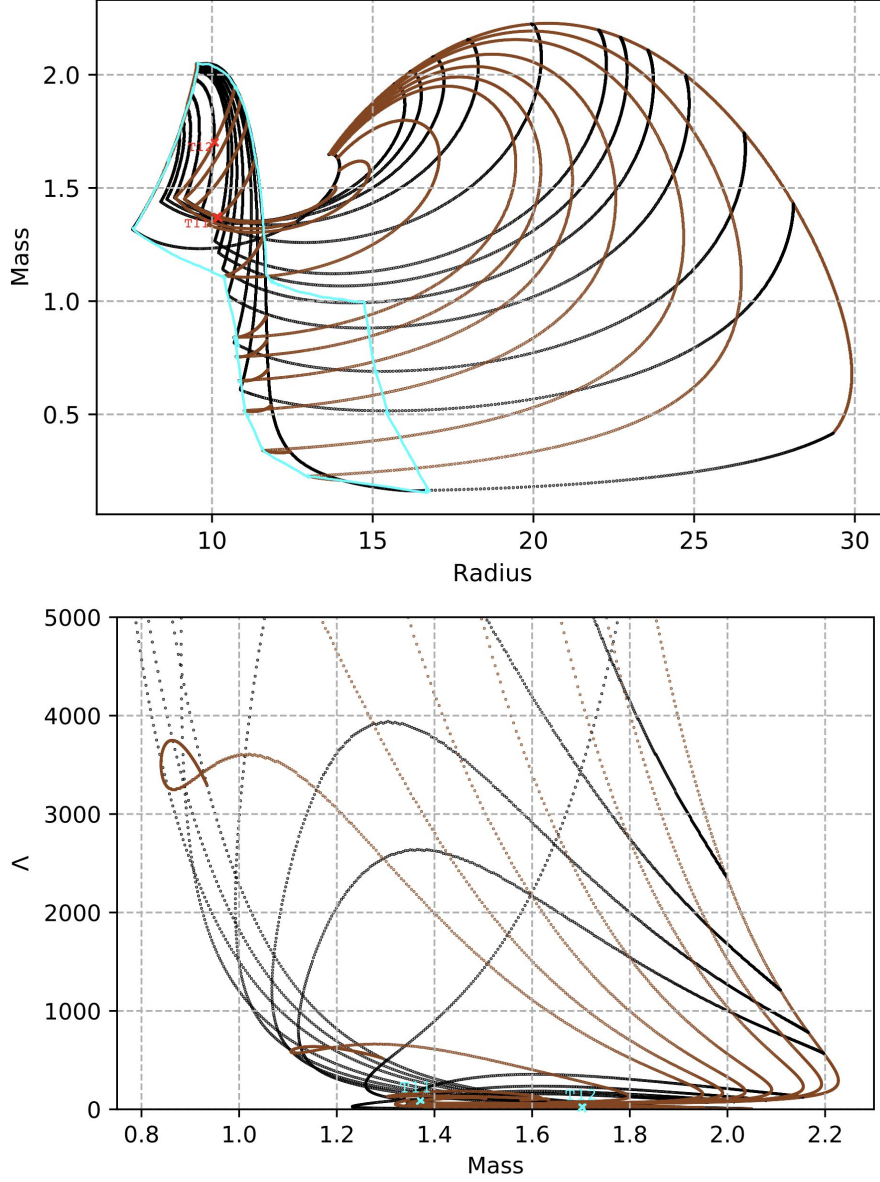


Figure 4: Mass-Radius (Up) and TLN-Mass (Down) relations and for the hybrid stars of type (IIIa) and (IIIb) in Fig. 1 for SLy4 EoS and for dark matter EoS with $\mathcal{B} = 0.055$. The region of stable configurations is specified by the aqua-encircled area. Different black lines correspond to different core pressures of dark matter but varying the core pressures of the nuclear matter, and the brown lines are the other way around. The crosses (two red ones in the up panel and two aqua ones in the down panel) indicate special stars T11 and T12 mentioned later in Table 1.

(reverse) BTM criteria.

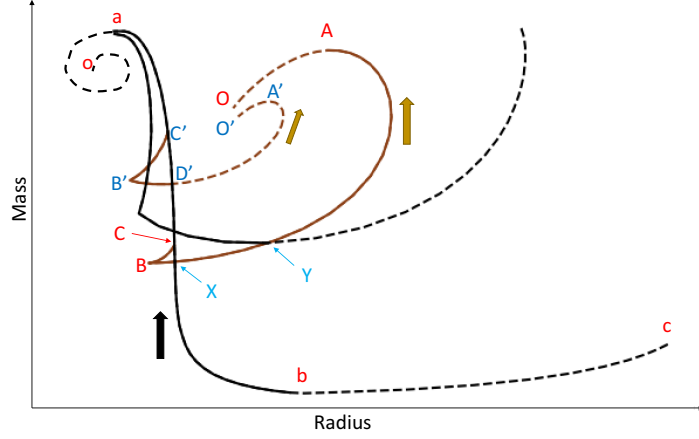


Figure 5: Some typical examples for the stability regimes of the M - R curve of the third scenario hybrid stars. The black curves are NS-like and the brown curves are DM-like, which are defined in the main text. The block arrows indicate the directions of increasing of the core pressures. We use the (reverse) BTM criteria discussed in the main text to determine the stable/unstable regimes, which are indicated by solid/dotted parts. A caveat for the intersection point is as follows. Since the mass and radius depend on both the core pressures of nuclear and dark matters, some of the intersection points may be the faked ones and cannot be used to judge the saddle (in)stability. For examples, the intersection points C and Y are real ones, while the point X is a fake intersection point. For more details, see the main text.

Moreover, in the third scenario of hybrid stars, we have two orthogonal ways of changing the core pressures, and thus arrive at two sets of M - R curves. One set called NS-like is to fix the core pressure of dark matter but change the one of the nuclear matter, and the other one called DM-like is the other way around. A typical example is shown in Fig. 5, where the black curves are NS-like and the brown curves are DM-like. We apply the above (reverse) BTM criteria to determine the stability/instability regime of each curve, then look for the regimes where both NS-like and DM-like curves admit stability. These regimes will then be identified as the stable hybrid stars of scenario III. However, there is one caveat. In Fig. 5 we see that one brown curve may intersect one black curve twice, for example, the C and X on the curve O - A - B - C . Since on the same black curve, the core pressure of the dark matter part is fixed, so one of them will be the fake intersection point. In this case, X is not the “real” intersection point since C is the starting point at which the core pressure of the dark matter equal to the one on the black curve. Thus, the intersection point X will not be used to judge the saddle stability. Another subtle issue is if there is a change of stability around the sharp edge points such as B and B' at which a first order phase transition from a nuclear crust to a dark crust may happen. Notice that the rotation directions before and after such points are opposite (from clockwise to counterclockwise) thus the BTM criteria cannot be applied, and B' is not even an extremum. In (Alford et al. 2017) it was shown that there is a stability change around such points. More rigorous derivation is needed for the future study. However, due to the fact that B' - D' and B - A are already stable, C' - D' and C - B shall be stable no matter if we adopt the criteria of (Alford et al. 2017).

By applying the lessons learned from the typical examples in Fig. 5, we can roughly

mark the stable regimes in Fig. 4 by the aqua-encircled areas. We see that the stable hybrid stars of the third scenario are limited to left parts of the M - R curves, which are more NS-like and can have the maximum masses comparable with the ones for pure neutron stars. However, there are no stable DM-like hybrid stars due to the saddle instability. One naive interpretation is because that a boson star with low central pressure like $10^{-6}p_{\odot}$ is stable, while a neutron star with the same central pressure is unstable. Thus, a hybrid star deviates a little from a pure neutron star can have a stable boson part with low boson central pressure. Moreover, as in the first two scenarios, our hybrid stars can feature a wider range of masses and TLNs than the pure neutron stars of a given EoS.

Even there are still uncertainties for the EoS of nuclear matter which may hinder our above interpretations, it is still interesting to demonstrate the capability of our hybrid stars with a given nuclear matter EoS, i.e., SLy4, to interpret the observed GW events such as GW190425. The full picture by pinning down the uncertainties for both nuclear and dark matters should be expected from the PE of the coming GW events.

Index	Type	M	M_D/M	R	R_D	R_N	Λ
T1	aRD	1.37	0	11.59	0		360
T2	aRD	1.37	0.07	11.96	4.5		486
T3	aRD	1.9	0.65	10.77	8		21
T4	aRD	1.7	0.26	13.19	8		352
T5	aRD	1.5	0.21	13.54	8		999
T6	aRD	3.42	0.93	26.91	25		1802
T7	aRN	1.7	0.15	12.90		10.7	79
T8	aRN	3.5	1.0	33.34		0	390
T9	bRD	1.7	0.53	11.63	8		104
T10	bRN	1.7	0.01	11.97		10.7	77
T11	bMX	1.37	0.30	10.14	10.14	9.35	87
T12	bMX	1.7	0.11	10.06	7.62	10.06	25

Table 1: List of 12 specific hybrid stars, most of which are indicated on Fig. 2 and 4. The first entry labels the stars, and the second entry is the type of hybrid stars as defined earlier, then the subsequent entries are total mass, mass ratio of dark matter to the total mass, total radius, respective core radius and TLN. The core pressures of dark matter for T11 and T12 are $2.5 \times 10^{-4}p_{\odot}$ and $2.0 \times 10^{-4}p_{\odot}$, respectively.

5 Fitting of GW170817 and GW 190425

After discussing the general M - R and Λ - R relations for the three scenarios of compact hybrid stars, we now pick up some specific configurations as listed in Table 1 which can be identified as the component stars for the GW170817 and GW 190425. In Table 1 we have listed 12 hybrid stars labeled by the index Tn with $n=1 \dots 12$. Most of them are indicated on Fig. 2 and 4. The types **aRD**, **aRN**, **bRD**, **bRN** and **bMX** are defined as before to indicate the different choices of core radius and \mathcal{B} . Especially, we list T6 and T8 to show that the

typical high mass stars with mass larger than $3M_\odot$ are mainly the dark stars and cannot be the final states of the mergers of low mass hybrid stars mainly composed of nuclear matter. Besides, most of the stars with masses lower than $2M_\odot$ have radii just 2 or 3km larger than the typical radii of neutron stars, say around 11km. Some of them such as T7 and T10 yet have 10.7km neutron cores to be consistent with the observed photon radius (Lattimer & Steiner 2014; Cackett et al. 2008; Ozel et al. 2016).

Since $\tilde{\Lambda} = (\Lambda_1 + \Lambda_2)/2$ for the equal-mass binary, any two stars from the same type labelled by either **a** or **b**, e.g. two T2's, two T11's, or {T1, T2} etc, can form a binary of hybrid stars with $\tilde{\Lambda}$ close to it observational upper bound to explain GW170817.

In contrast, for GW190425 the inferred total mass $M_1 + M_2 \simeq 3.4^{+0.3}_{-0.1}M_\odot$, with $M_1 \in (1.62, 1.88)M_\odot$, $M_2 \in (1.45, 1.69)M_\odot$ and $\tilde{\Lambda} \leq 600$ for low spin prior, or with $M_1 \in (1.61, 2.52)M_\odot$, $M_2 \in (1.12, 1.68)M_\odot$ and $\tilde{\Lambda} \leq 1100$ for high-spin prior (Abbott et al. 2020a). From Table 1, we can find the following pairs of hybrid stars with SLy4 EoS to explain GW190425: (1) two T4's with $\tilde{\Lambda} = 352$, (2) {T3, T5} with $\tilde{\Lambda} = 348$, (3) two T7's with $\tilde{\Lambda} = 79$, (4) two T9's with $\tilde{\Lambda} = 104$, (5) two T10's with $\tilde{\Lambda} = 77$ and (6) two T12's with $\tilde{\Lambda} = 25$. From Table 1 it is interesting to see that the values of Λ cover a wide range, even with the same masses.

Note that for GW170817, the inferred total mass $M_1 + M_2 \simeq 2.73^{+0.04}_{-0.01}M_\odot$ with $M_1 \in (1.36, 1.60)M_\odot$, $M_2 \in (1.16, 1.36)M_\odot$ and $\tilde{\Lambda} = 300^{+420}_{-230}$ for low-spin prior. For simplicity, we consider the equal mass pair with $M_1 = M_2 = 1.37M_\odot$ (Abbott et al. 2017, 2019). The pure-neutron or hybrid stars with such mass in the list are T1, T2 and T11. In this set, unlike T11 which belongs to the third scenario, T1 and T2 belong to the first two scenarios and have none or little dark matter.

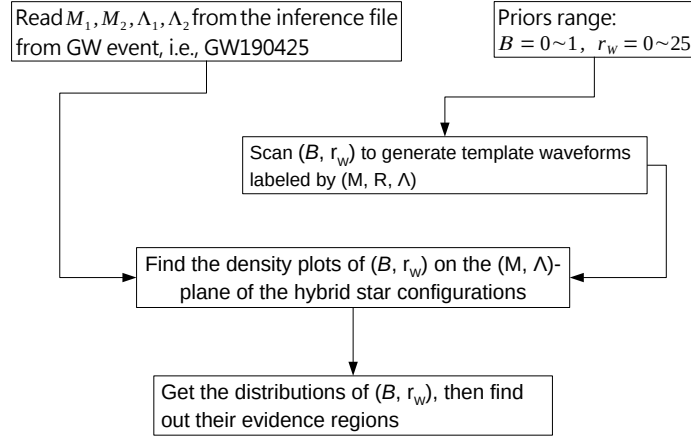


Figure 6: Flow chart of obtaining posteriors of model parameters for the hybrid stars from the posteriors of PE for a particular GW event, such as GW190425. See the main text for more detailed explanation.

6 Parameter estimation for EoS of dark matter

Finally, we would like to demonstrate that one can use the GW data and the associated parameter estimation (PE) results to obtain the posteriors of the EoS parameter. For simplicity, we will consider the first two scenarios of hybrid stars made of the nuclear matter

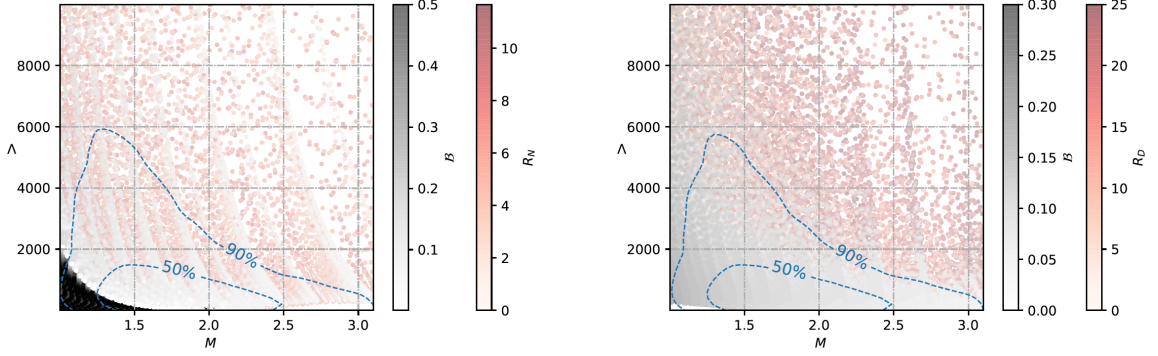


Figure 7: Density plots of parameters (\mathcal{B}, r_W) on the (M, Λ) -plane of the hybrid star configurations of scenario I (Left panel, with $r_W = R_N$) and II (Right panel, with $r_W = R_D$). The side bars indicate the scales of the density plots. There is no hybrid star configurations falling inside the corresponding (M, Λ) regions when (\mathcal{B}, r_W) go beyond the maximal values of the side bars. The credible intervals of 50% and 90% of the PE results for GW190425 are indicated by the blue dashed lines (Vallisneri et al. 2015).

with SLy4 EoS and bosonic SIDM with EoS given by (1). The details of the Mass-Radius and TLN-Mass relations are already obtained in section 4. We then try to map the PE posteriors of GW190425 to the posteriors of the EoS parameter $\mathcal{B} \sim \frac{0.08}{\sqrt{\Lambda}} \left(\frac{m}{\text{GeV}}\right)^2$ and the core radius r_W .

The key procedure of the PE goes as follows: (1) obtaining the sample bank of the posteriors for $M_{1,2}$ and $\Lambda_{1,2}$ from (Abbott et al. 2020a); (2) obtaining the bank of $M_{1,2}$ and $\Lambda_{1,2}$ from solving TOV and then evaluating TLNs by finely tuning \mathcal{B} and r_W ; (3) matching the bank of (1) to the bank of (2) to obtain the density plots of \mathcal{B} and r_W and thus their posteriors. The flow chart for the above procedure of mapping the posteriors of GW190425 to the posteriors of hybrid star properties is shown in Fig. 6.

Start the the procedure of the flow chart by giving the prior range of $\mathcal{B} = [0, 1]$ and $r_W = [0, 25]$. Within the ranges, we generate the template waveforms labelled by the mass, radius and TLN. Next, combining the above with the PE headcounts of the sample inference file for GW190425, we generate the density plots of (\mathcal{B}, r_W) on the (M, Λ) -plane of the hybrid star configurations of scenario I ($r_W = R_N$) and II ($r_W = R_D$). The results are shown in Fig. 7 for scenario I (top panel) and II (bottom panel). Based on these density plots, we further map the PE headcounts labelled by $[M_1, M_2, \Lambda_1, \Lambda_2]$ to the ones labelled by (\mathcal{B}, r_W) . In this way we can map the posteriors of (M, Λ) to the posteriors of (\mathcal{B}, r_W) . The results are shown in Fig. 8. The inferred best-fitted values are $\mathcal{B} = 0.07_{-0.02}^{+0.09}$ and $\mathbf{RN} = 6.44_{-2.85}^{+1.98}$ km for the scenario I, and $\mathcal{B} = 0.05_{-0.02}^{+0.04}$ and $\mathbf{RD} = 10.29_{-4.10}^{+3.49}$ km for the scenario II. Together with the astrophysical constraint (2), we can infer the parameters of SIDM and obtain $\lambda \in (131, 3076)$ and $m \in (2.68, 10.53)$ GeV for the first scenario, and $\lambda \in (71, 1542)$ and $m \in (1.78, 6.65)$ GeV for the second scenario. Both satisfy well the constraint $\lambda M_{\text{plank}}^2 / m^2 \gg 1$. Further GW data is expected to sharpen the above estimation.

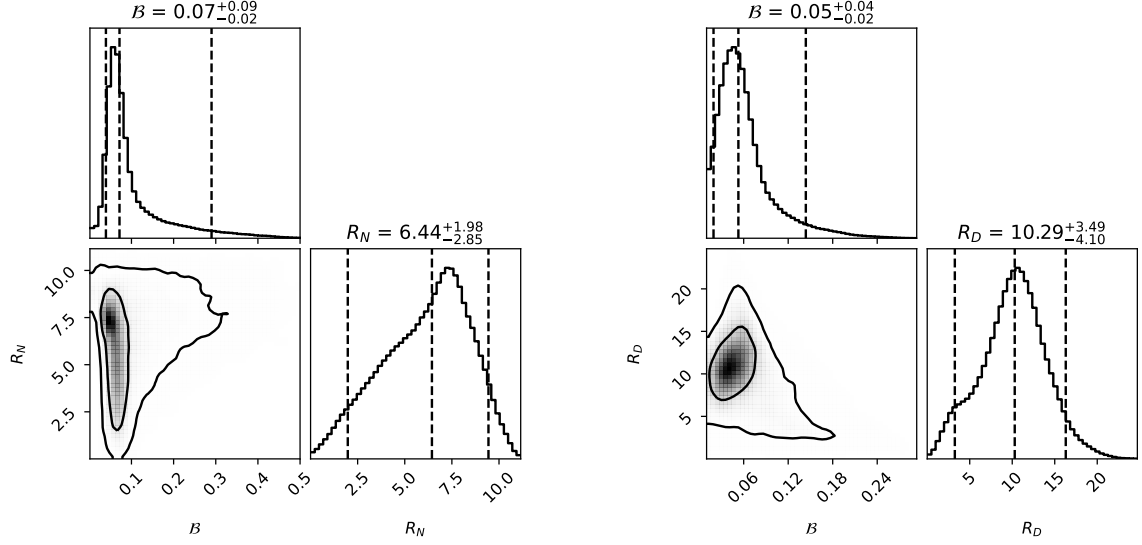


Figure 8: Posteriors for the dark matter EoS parameter \mathcal{B} (horizontal axis) of the SIDM and the core-radius r_W (vertical axis) for the first (left sub-figure) and the second (right sub-figure) scenarios with neutron SLy4 EoS. The inner circled regions are 50% credible interval, and the outer ones are 90% credible interval. The inferred best-fitted values of \mathcal{B} and r_W are also given in the main text.

7 Conclusion

Dark matter has an abundance much higher than that of normal matter, though the self-interaction of dark matter is considered to be weak, we cannot exclude the possibility for it to form compact objects like dark stars. The lack of traditional astronomical observations of dark stars on the contrary indicates the importance of GW events as probes for them. Therefore, we examine the GW properties of dark or hybrid stars by assuming their existence, rather than ruling them out for granted. We choose some special EoSs for neutrons and dark bosons in this paper, but the method we develop here can be applied to any EoS. That means, any compact star with two or more components can be discussed using our model.

In this paper we have shown that it is possible to explain some GW events such as GW170817 and GW190425 by our hybrid star scenarios. There remain uncertainties for the EoS of nuclear matter which may hinder the hybrid star identifications. However, for a given EoS of nuclear matter, the possible configurations on the mass-radius and mass-TLN diagrams are broader than the given pure neutron star configurations. This should be true even taking into account the uncertainties of EoS for nuclear matter. Therefore, we expect the dark/hybrid star scenarios should be pinned down or ruled out by the future GW observations, especially when the interpretation of the exotic compact objects is needed.

Our study integrates three areas: gravitational waves, astronomy and particle physics. The vision becomes more clear than confined in a single subject. From our results, we see that a hybrid star can have a mass higher than the maximal mass of the neutron stars for a given EoS of nuclear matter. Moreover, the visible neutron core of this heavier hybrid star could still be comparable to the radius of the corresponding neutron star even if its total size is far larger than its core size. This then opens a possibility to lower/relax the maximal mass requirement for a nuclear EoS, and at the same time is able to interpret the heavier

mass compact object as a hybrid star when its mass is higher than the maximal mass of a conventional neutron star. A recent example is the companion star in GW190814, which has a mass of $2.6M_{\odot}$. This is larger than the conventional neutron star's maximal mass about $2.5M_{\odot}$. Our hybrid star scenario can easily explain GW190814 as well as the other two possible BNS/BHS events GW170817 and GW190425.

Acknowledgement

FLL and GZH are supported by Taiwan Ministry of Science and Technology (MoST) through Grant No. 106-2112-M-003-004-MY3. KZ (Hong Zhang) is supported by MoST through Grant No. 107-2811-M-003-511. We thank Yen-Hsun Lin, Alessandro Parisi and other TGWG members for helpful discussions. We also thank NCTS for partial financial support.

References

- Abbott, B. et al. 2017, Phys. Rev. Lett., 119, 161101
- Abbott, B. et al. 2019, Phys. Rev. X, 9, 011001
- Abbott, B. et al. 2020a, Astrophys. J. Lett., 892, L3
- Abbott, R. et al. 2020b, Astrophys. J. Lett., 896, L44
- Akerib, D. et al. 2017, Phys. Rev. Lett., 118, 021303
- Alford, M. G., Harris, S. P., & Sachdeva, P. S. 2017, Astrophys. J., 847, 109
- Annala, E., Ecker, C., Hoyos, C., et al. 2018, JHEP, 12, 078
- Aprile, E. et al. 2017, Phys. Rev. Lett., 119, 181301
- Bardeen, J. M., Thorne, K. S., & Meltzer, D. W. 1966, apj, 145, 505
- Battaglia, G., Helmi, A., Morrison, H., et al. 2005, Mon. Not. Roy. Astron. Soc., 364, 433, [Erratum: Mon.Not.Roy.Astron.Soc. 370, 1055 (2006)]
- Cackett, E. M., Miller, J. M., Bhattacharyya, S., et al. 2008, Astrophys. J., 674, 415
- Colpi, M., Shapiro, S., & Wasserman, I. 1986, Phys. Rev. Lett., 57, 2485
- Coskuner, A., Grabowska, D. M., Knapen, S., & Zurek, K. M. 2019, Phys. Rev. D, 100, 035025
- Cui, X. et al. 2017, Phys. Rev. Lett., 119, 181302
- Deliyergiyev, M., Del Popolo, A., Tolos, L., et al. 2019, Phys. Rev. D, 99, 063015
- Douchin, F. & Haensel, P. 2001, Astron. Astrophys., 380, 151
- Eby, J., Kouvaris, C., Nielsen, N. G., & Wijewardhana, L. 2016, JHEP, 02, 028

- Eby, J., Leembruggen, M., Street, L., Suranyi, P., & Wijewardhana, L. R. 2019, *Phys. Rev. D*, 100, 063002
- Edgar, R. G. 2004, *New Astron. Rev.*, 48, 843
- Ellis, J., Hütsi, G., Kannike, K., et al. 2018, *Phys. Rev. D*, 97, 123007
- Gresham, M. I., Lou, H. K., & Zurek, K. M. 2017, *Phys. Rev. D*, 96, 096012
- Gresham, M. I., Lou, H. K., & Zurek, K. M. 2018a, *Phys. Rev. D*, 98, 096001
- Gresham, M. I., Lou, H. K., & Zurek, K. M. 2018b, *Phys. Rev. D*, 97, 036003
- Gresham, M. I. & Zurek, K. M. 2019, *Phys. Rev. D*, 99, 083008
- Hannuksela, O. A., Wong, K. W., Brito, R., Berti, E., & Li, T. G. 2019, *Nature Astron.*, 3, 447
- Hata, H., Sakai, T., Sugimoto, S., & Yamato, S. 2007, *Prog. Theor. Phys.*, 117, 1157
- Hinderer, T. 2008, *Astrophys. J.*, 677, 1216
- Hoyos, C., Rodríguez Fernández, D., Jokela, N., & Vuorinen, A. 2016, *Phys. Rev. Lett.*, 117, 032501
- Jungman, G., Kamionkowski, M., & Griest, K. 1996, *Phys. Rept.*, 267, 195
- Kaplinghat, M., Tulin, S., & Yu, H.-B. 2016, *Phys. Rev. Lett.*, 116, 041302
- Klasen, M., Pohl, M., & Sigl, G. 2015, *Prog. Part. Nucl. Phys.*, 85, 1
- Kouvaris, C. & Nielsen, N. G. 2015, *Phys. Rev. D*, 92, 063526
- Kouvaris, C. & Tinyakov, P. 2011, *Phys. Rev. D*, 83, 083512
- Kuster, M., Raffelt, G., & Beltran, B., eds. 2008, *Axions: Theory, cosmology, and experimental searches. Proceedings, 1st Joint ILIAS-CERN-CAST axion training, Geneva, Switzerland, November 30-December 2, 2005, Vol. 741, pp.1–258*
- Lattimer, J. M. & Steiner, A. W. 2014, *Astrophys. J.*, 784, 123
- Maselli, A., Pnigouras, P., Nielsen, N. G., Kouvaris, C., & Kokkotas, K. D. 2017, *Phys. Rev. D*, 96, 023005
- McDermott, S. D., Yu, H.-B., & Zurek, K. M. 2012, *Phys. Rev. D*, 85, 023519
- Mukhopadhyay, S., Atta, D., Imam, K., Basu, D., & Samanta, C. 2017, *Eur. Phys. J. C*, 77, 440, [Erratum: *Eur.Phys.J.C* 77, 553 (2017)]
- Nelson, A., Reddy, S., & Zhou, D. 2019, *JCAP*, 07, 012
- Oppenheimer, J. & Volkoff, G. 1939, *Phys. Rev.*, 55, 374
- Ozel, F., Psaltis, D., Guver, T., et al. 2016, *Astrophys. J.*, 820, 28

- Peter, A. H., Rocha, M., Bullock, J. S., & Kaplinghat, M. 2013, *Mon. Not. Roy. Astron. Soc.*, 430, 105
- Postnikov, S., Prakash, M., & Lattimer, J. M. 2010, *Phys. Rev. D*, 82, 024016
- Rezaei, Z. 2018, *Int. J. Mod. Phys. D*, 27, 1950002
- Rocha, M., Peter, A. H., Bullock, J. S., et al. 2013, *Mon. Not. Roy. Astron. Soc.*, 430, 81
- Sakai, T. & Sugimoto, S. 2005a, *Prog. Theor. Phys.*, 113, 843
- Sakai, T. & Sugimoto, S. 2005b, *Prog. Theor. Phys.*, 114, 1083
- Schunck, F. E. & Mielke, E. W. 2003, *Class. Quant. Grav.*, 20, R301
- Sennett, N., Hinderer, T., Steinhoff, J., Buonanno, A., & Ossokine, S. 2017, *Phys. Rev. D*, 96, 024002
- Spergel, D. N. & Steinhardt, P. J. 2000, *Phys. Rev. Lett.*, 84, 3760
- Tolman, R. C. 1939, *Phys. Rev.*, 55, 364
- Vallisneri, M., Kanner, J., Williams, R., Weinstein, A., & Stephens, B. 2015, *J. Phys. Conf. Ser.*, 610, 012021
- Zhang, K., Hirayama, T., Luo, L.-W., & Lin, F.-L. 2020, *Phys. Lett. B*, 801, 135176
- Zhang, K. & Lin, F.-L. 2020, *Universe*, 6, 231